

Electronic Supplementary Information for

Pillar[5]arene-Based Covalent Organic Framework with Pre-encoded Selective Host-guest Recognition

Lu Liu,^{a,c} Yiming Hu,^c Shaofeng Huang,^c Yinghua Jin,^c Jingnan Cui,^a Weitao Gong,^{* a,b} Wei Zhang^{* c}

^a. State Key Laboratory of Fine Chemicals, School of Chemical Engineering, Dalian University of Technology, Dalian 116024, P. R. China.

^b. Engineering Laboratory of Boric and Magnesium Functional Material Preparative and Applied Technology, Dalian, Liaoning Province, 116024, P. R. China.

^c. Department of Chemistry, University of Colorado Boulder, Boulder, Colorado 80309, United States.

1. Materials and general methods	2
2. Experimental procedures	3
Scheme S1. Synthetic scheme of APP5	3
Synthesis of compound APP5:	3
Fig. S1 ¹ H NMR spectrum of compound APP5	4
Fig. S2 ¹³ C NMR spectrum of compound APP5	4
Synthesis of COFs	5
Synthesis of P5-COF.	5
Synthesis of Model-COF	5
Fig. S3 FT-IR spectra of TFB , APP5 , and P5-COF .	6
Fig. S4 FT-IR spectra of TFB , TP , and Model-COF .	6
Fig. S5 ¹³ C CP/MAS NMR spectrum of P5-COF .	7
Fig. S6 ¹³ C CP/MAS NMR spectrum of Model-COF .	7
Fig. S7 Thermogravimetric analysis of Model-COF and P5-COF	8
Fig. S8 SEM images of Model-COF and P5-COF .	8
Fig. S9 TEM images of P5-COF and Model-COF .	9
Fig. S10 PXRD analysis of Model-COF .	9
Fig. S11 PXRD pattern of P5-COF and Model-COF after immersed in different solution	10
Fig. S12 N ₂ Adsorption Isotherms of Model-COF .	10
Fig. S13 Top view and side view of Model-COF	11
Fig. S14 The pore size distribution of P5-COF and Model-COF .	11
Table S1. The pore properties of P5-COF and Model-COF	11
Standard Curve of UV adsorption vs. paraquat concentration:	12
Fig. S16 Stability test of P5-COF for Paraquat	12
Fig. S17 Gas adsorption isotherms of P5-COF and Model-COF	13
Table S2. Comparison of gas adsorption properties of P5-COF with other reported MOFs.	13
References:	13

1. Materials and general methods

All commercial chemicals are of analytical grade and were used without further purification. Compound **P5-OTf** and **APP5** were synthesized following previously reported procedures^{1,2}.

NMR spectra were taken on Bruker 300 and Inova 500 spectrometers. CHCl₃ (7.26 ppm) was used as an internal reference in ¹H NMR, and CDCl₃ (77.16 ppm) for ¹³C NMR spectra. NMR data is reported in the following order: chemical shift, multiplicity (s, singlet; d, doublet; t, triplet; q, quartet; m, multiplet), coupling constants (*J*, Hz), number of protons. Solid-state cross-polarization magic-angle spinning (CP/MAS) NMR spectra were recorded on an Inova 400 NMR spectrometer. Powder X-Ray Diffraction (PXRD) was obtained from Inel CPS 120 diffraction system, using monochromated Cu Kα (λ=1.542 Å) radiation.

The FT-IR spectra of starting materials and COFs were obtained from Agilent Technologies Cary 630 FT-IR. Thermogravimetric analyses (TGA) were performed on Mettler Toledo TGA/DSC3+ instrument by heating the samples under nitrogen atmosphere at a heating rate of 5 °C min⁻¹ within the temperature range of 30-800 °C.

The Quantachrome Autosorb ASiQ automated gas sorption analyzer was used to measure N₂ adsorption isotherm. The samples were heated at 120 °C and kept at this temperature for 24 h under vacuum for activation. Ultra high purity grade (99.999% purity) N₂, C₂H₂, C₂H₄, C₂H₆, and gas regulators were used for all free space corrections and measurements. For the gas adsorption measurement, the temperatures were controlled by using a refrigerated bath of liquid N₂ (77 K), ice water (273K) and water (295 K). The pore size distribution was calculated with quenched solid density functional theory (QSDFT) and cylindrical pore model based on the nitrogen sorption isotherms at 77 K using Quantachrome AsiQwin program. The morphology of the samples were characterized by a Tescan Vega3 scanning electron microscope (SEM).

Adsorption capacity:

The polymer was added into H₂O of paraquat (3 mL) with an initial concentration of 0.06 mM, 0.07 mM, 0.08 mM, 0.09 mM, 0.1 mM, 0.16 mM, and 0.2 mM. The suspension was stirred for 12 h and then filtered. The concentration of paraquat in the

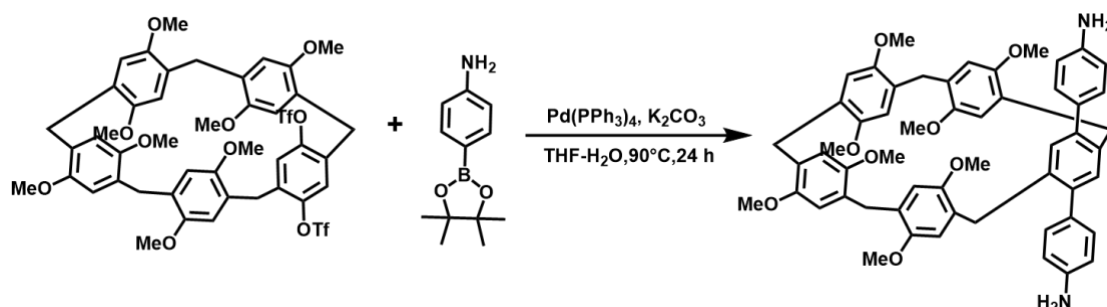
filtrate was determined with UV-Vis spectroscopy (257 nm).

The adsorption data were fitted with Langmuir isotherm model using the following equation:

$$q_e = \frac{q_{max}bc_e}{1 + bc_e}$$

Where q_e (mg g^{-1}) is the amount of pollutant adsorbed at equilibrium, C_e (mM) is the residual pollutant concentration at equilibrium, q_{max} (mg g^{-1}) is the maximum adsorption capacity of pollutants, and b is the equilibrium constant.

2. Experimental procedures



Scheme S1. Synthetic scheme of **APP5**.

Synthesis of compound **APP5**:

P5-OTf (1.70 g, 2.0 mmol), 4-aminophenylboronic acid pinacol ester (0.99 g, 4.5 mmol), potassium carbonate (2.76 g, 20 mmol), $\text{Pd}(\text{PPh}_3)_4$ (0.15 g, 0.1 mmol) and H_2O (10 mL) were dispersed in THF (40 mL). The mixture was degassed with nitrogen and stirred at 90°C overnight. The mixture was concentrated under reduced pressure, then purified by column chromatography to get **APP5** as a white powder (1.04 g, 60.0%): ^1H NMR (400 MHz, CDCl_3 , 298K) δ 6.93 (s, 2H), 6.79 (d, $J = 8.1$ Hz, 4H), 6.72 (d, $J = 9.9$ Hz, 4H), 6.55 (s, 2H), 6.48 (d, $J = 8.4$ Hz, 4H), 5.94 (s, 2H), 3.91-3.87 (m, 4H), 3.81-3.74 (m, 6H), 3.68 (s, 6H), 3.61-3.56 (m, 4H), 3.53 (s, 6H), 3.39 (s, 6H), 3.35 (s, 6H); ^{13}C NMR (75 MHz, CDCl_3) δ 150.95, 150.81, 150.67, 150.48, 144.91, 139.80, 136.46, 132.68, 132.34, 114.64, 114.25, 114.14, 114.09, 113.62, 56.03, 55.99, 55.73, 55.48, 33.07, 29.73, 29.25; HRMS: m/z calcd. for $[\text{M}+\text{H}]^+$ $\text{C}_{55}\text{H}_{57}\text{N}_2\text{O}_8$:873.4115; found 873.4114.

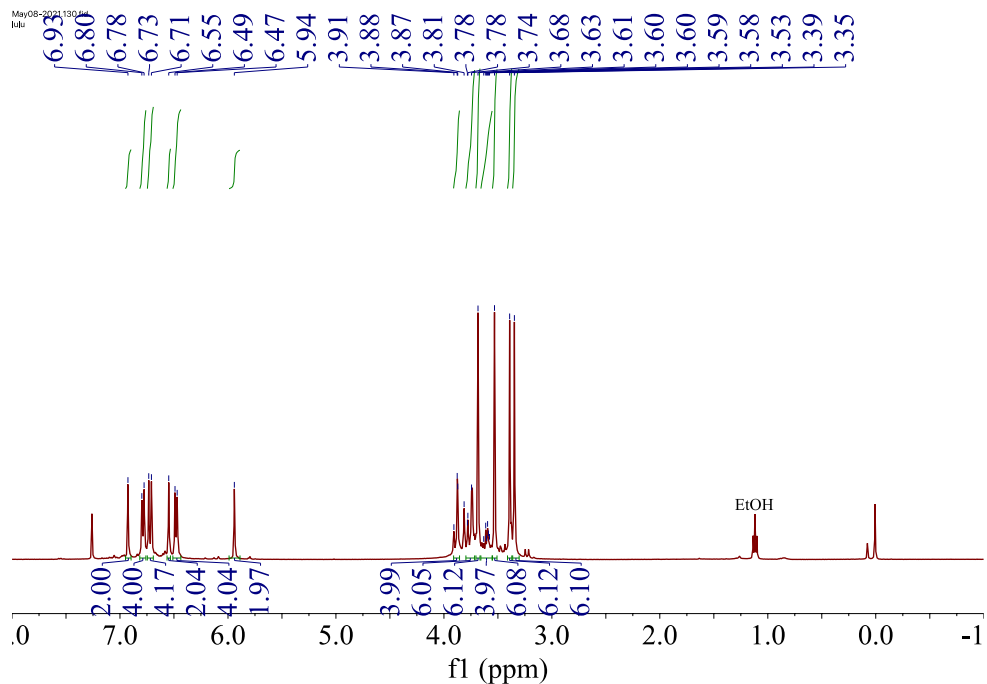


Fig. S1 ^1H NMR spectrum of compound **APP5** in CDCl_3 on 400 MHz.

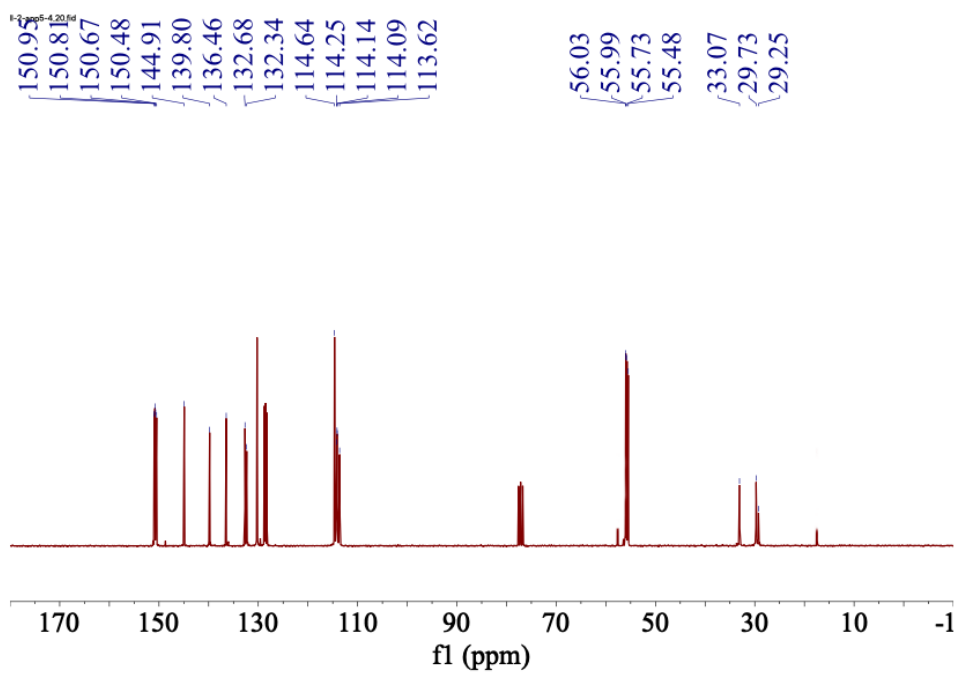


Fig. S2 ^{13}C NMR spectrum of compound **APP5** in CDCl_3 on 75 MHz.

Synthesis of COFs.

Synthesis of P5-COF.

An ampule was charged with 1,3,5-triformylbenzene (**TFB**) (8.0 mg, 0.050 mmol) and **APP5** (65 mg, 0.075 mmol) in a mixture of dioxane (0.10 mL), mesitylene (0.90 mL), and an aqueous solution of AcOH (0.20 mL, 6 M). The ampule was frozen at 77 K in liquid nitrogen and evacuated to the internal pressure of ~100 mTorr. Then the ampule was sealed with flame and heated at 120 °C for 3 days without any stirring and disturbance. The precipitate was collected by vacuum filtration, washed with THF under Soxhlet extraction for 48 h and further dried in vacuum at 120 °C. **P5-COF** was obtained as a yellow powder (57 mg, 78%): Anal. Calcd for **P5-COF** ($C_{384}H_{360}N_{12}O_{48}$)_n: C, 78.03; H, 6.14; N, 2.84; Found: C, 76.38; H, 6.08; N, 3.00.

Synthesis of Model-COF

An ampule was charged with 1,3,5-triformylbenzene (**TFB**) (8.0 mg, 0.050 mmol) and 4,4'-Diamino-*p*-terphenyl (**TP**) (20 mg, 0.075 mmol) in a mixture of dioxane (0.50 mL), mesitylene (0.50 mL), and an aqueous solution of AcOH (0.20 mL, 6 M). The ampule was frozen at 77 K in liquid nitrogen and evacuated to the internal pressure of ~100 mTorr. Then the ampule was sealed with flame and heated at 120 °C for 3 days without any stirring and disturbance. The precipitate was collected by vacuum filtration, washed with THF under Soxhlet extraction for 48 h, and further dried under vacuum at 120 °C. **Model-COF** was obtained as a yellow powder (18 mg, 63%): Anal. Calcd for **Model-COF** ($C_{163}H_{123}N_{12}$)_n: C, 87.02; H, 5.51; N, 7.47 Found: C, 82.01; H, 5.12; N, 7.66.

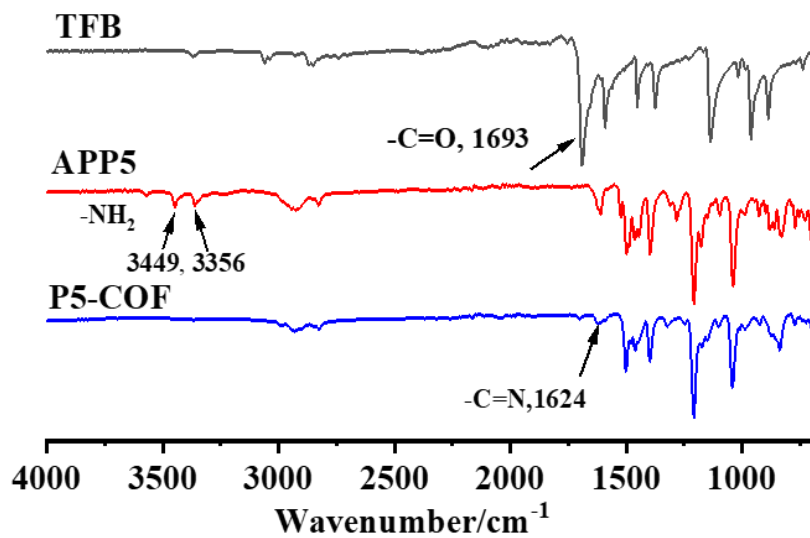


Fig. S3 FT-IR spectra of TFB (black), APP5 (red), and P5-COF (blue).

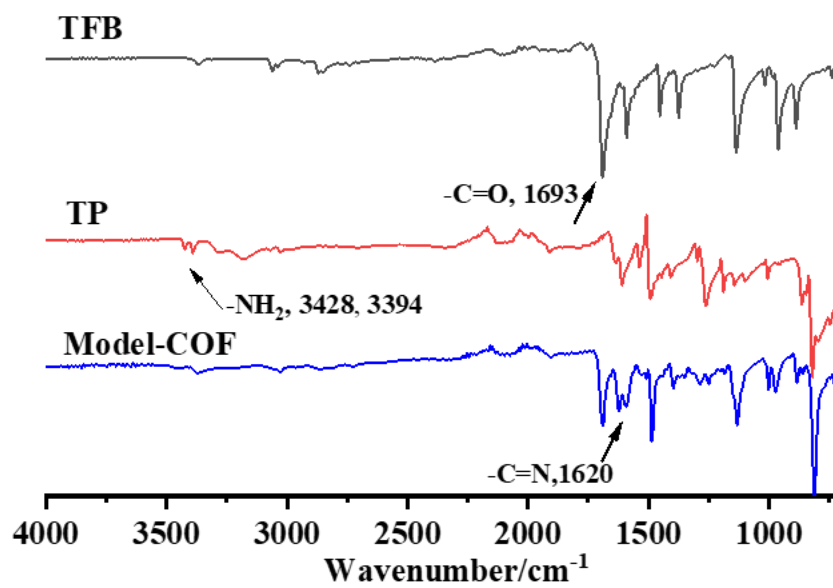


Fig. S4 FT-IR spectra of TFB (black), TP (red), and Model-COF (blue).

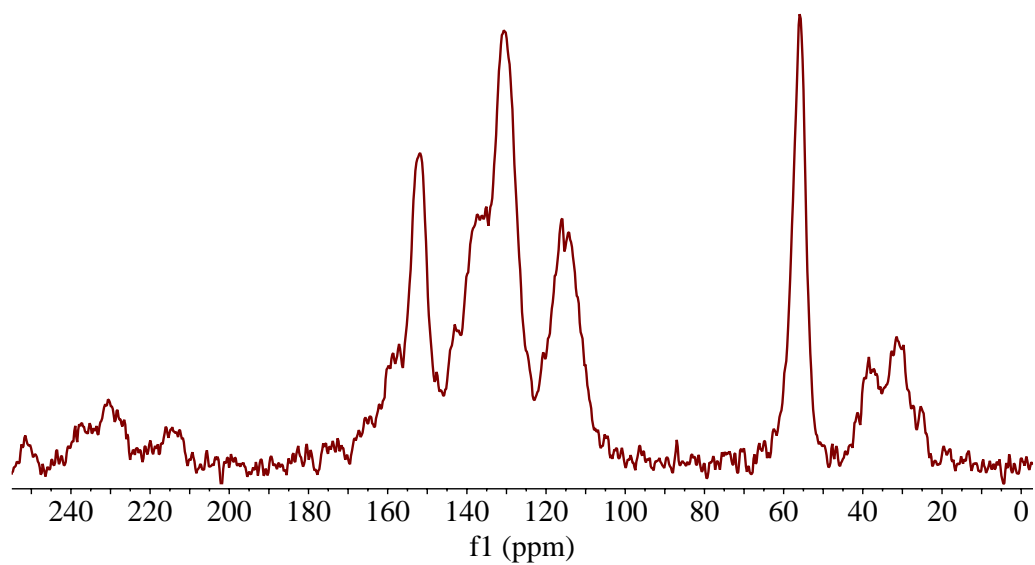


Fig. S5 ^{13}C CP/MAS NMR spectrum of **P5-COF**.

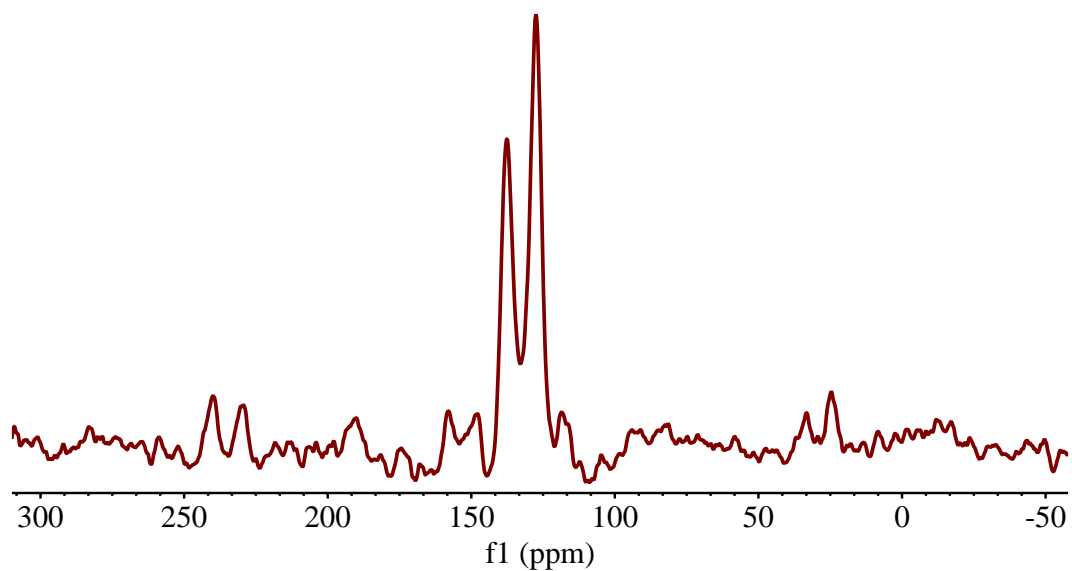


Fig. S6 ^{13}C CP/MAS NMR spectrum of **Model-COF**.

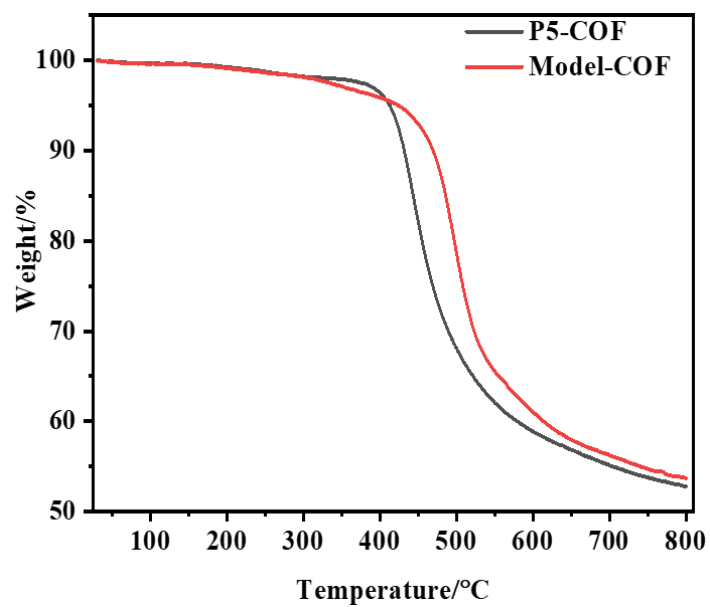


Fig. S7 Thermogravimetric analysis of **Model-COF** (red) and **P5-COF** (black) networks under N_2 atmosphere.

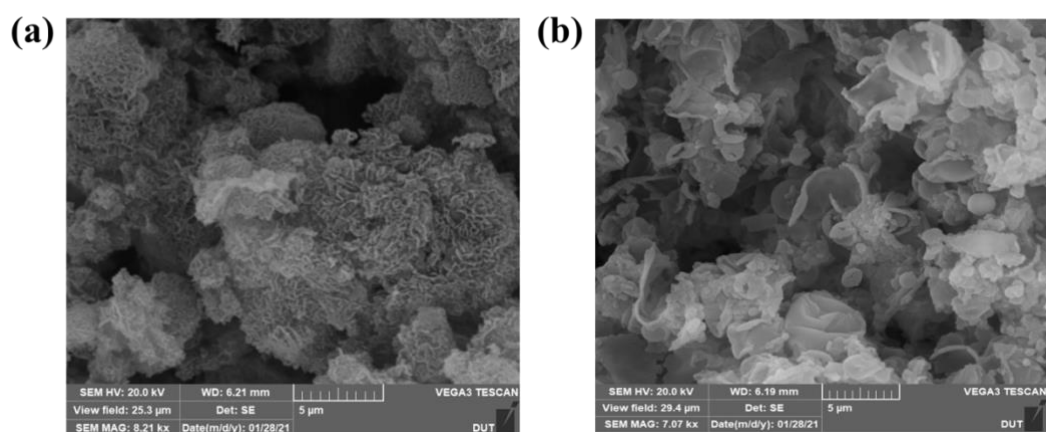


Fig. S8 SEM images of **Model-COF** (a) and **P5-COF** (b).

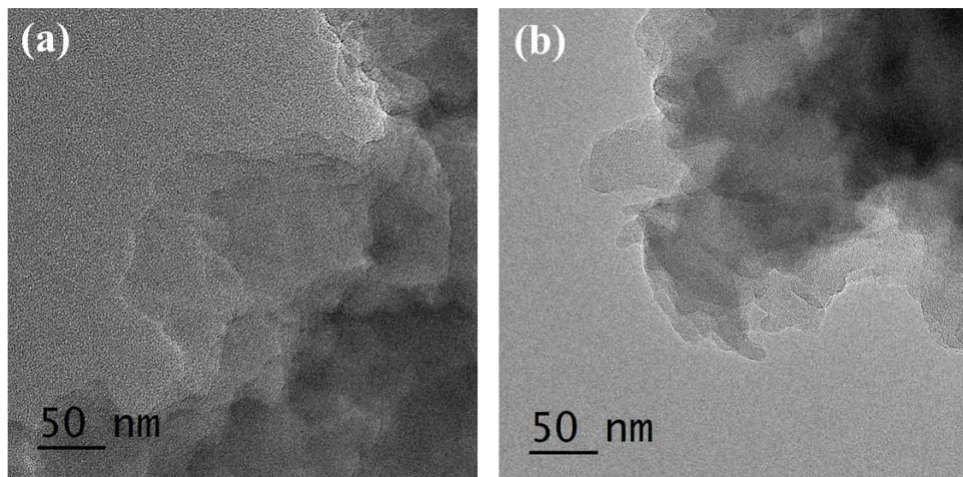


Fig. S9 TEM images of P5-COF (a) and Model-COF (b).

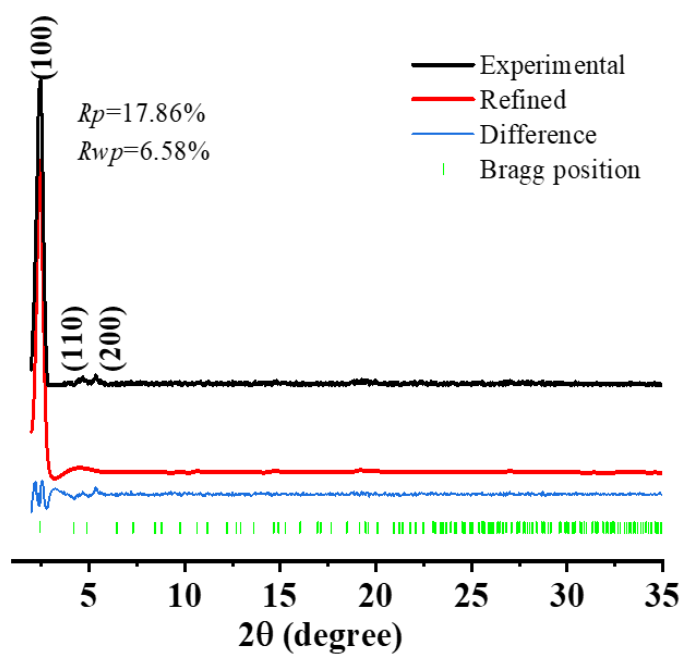


Fig. S10 PXRD analysis of Model-COF.

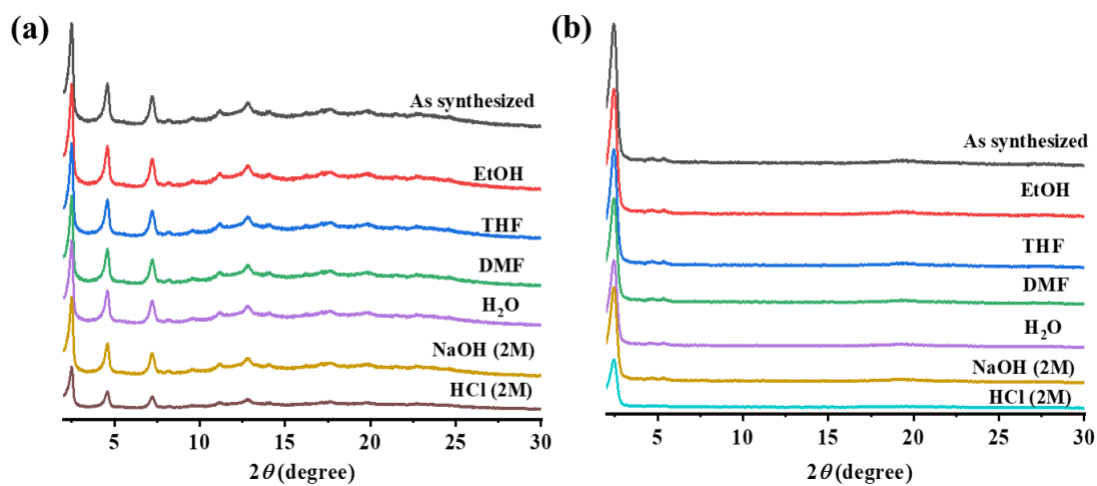


Fig. S11 PXRD pattern of **P5-COF** (a) and **Model-COF** (b) after immersed in different solution for 24h.

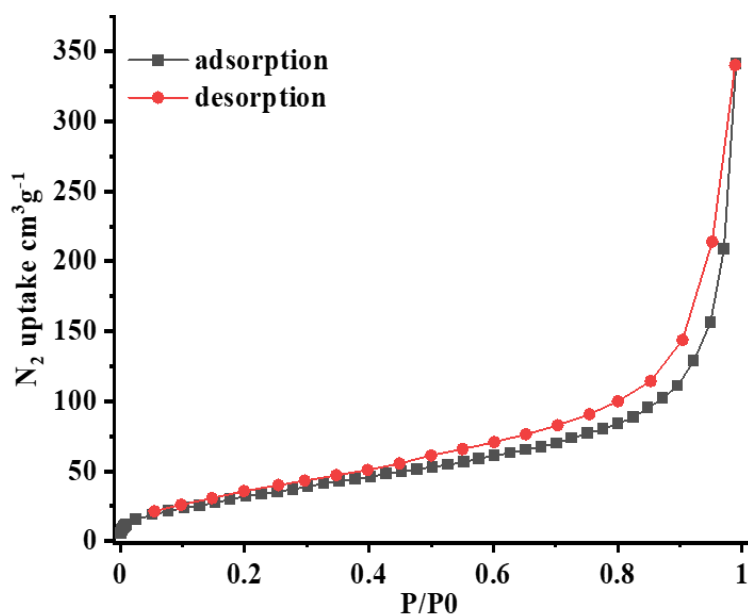


Fig. S12 N_2 Adsorption Isotherms of **Model-COF**.

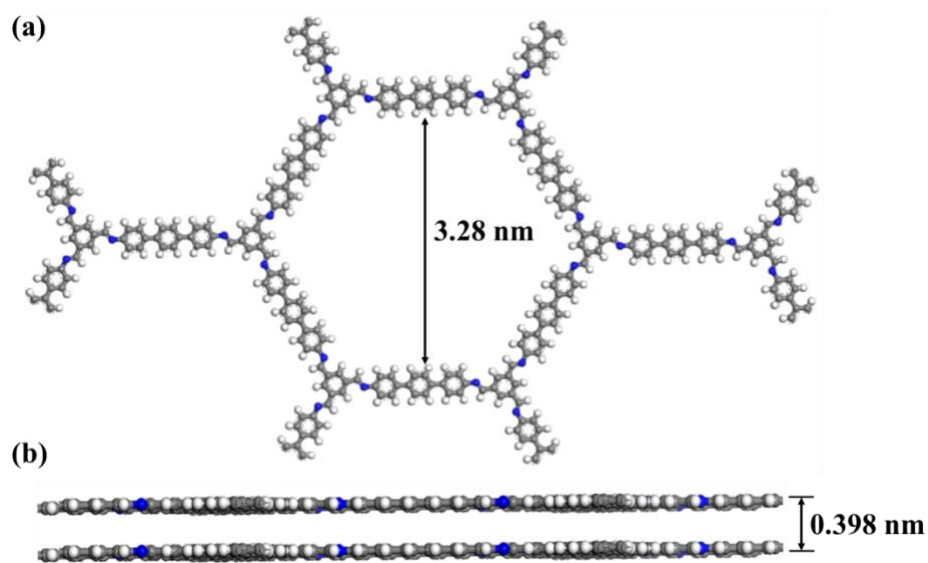


Fig. S13 Top view (a) and side view (b) of **Model-COF** in AA stacking model.

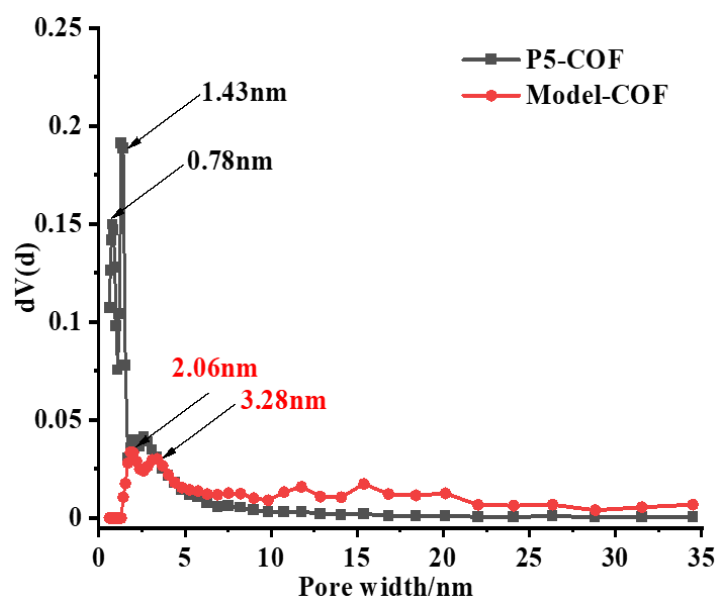


Fig. S14 The pore size distribution of **P5-COF** and **Model-COF**.

Table S1. The porosity of **P5-COF** and **Model-COF**.

Sample	S_{BET} ($\text{m}^2 \text{g}^{-1}$)	S_{Micro} ($\text{m}^2 \text{g}^{-1}$)	V_{Micro} ($\text{cm}^3 \text{g}^{-1}$)	V_{Total} ($\text{cm}^3 \text{g}^{-1}$)	Pore size (nm)
Model-COF	134.0	0	0	0.53	2.06/3.28
P5-COF	380.0	139.2	0.063	0.32	0.78/1.43

Calibration curve of UV adsorption vs. paraquat concentration:

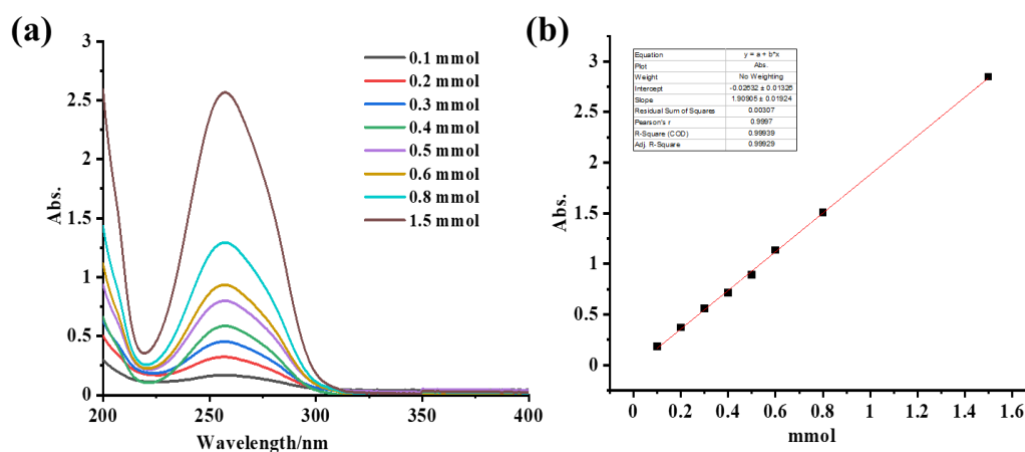


Fig. S15 UV-Vis spectra of paraquat at different concentrations (a); Calibration curve plotted based on the absorbance at 257 nm (b).

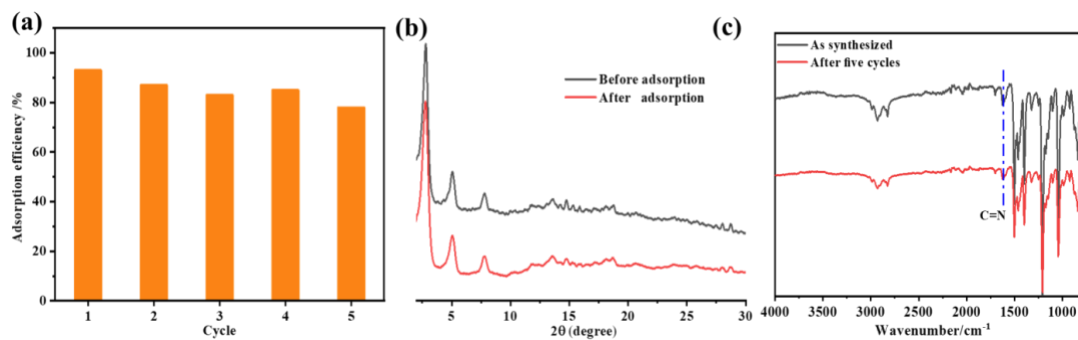


Fig. S16 (a) Recyclability of P5-COF for paraquat adsorption, (b) PXRD pattern of P5-COF before and after five cycles of adsorption study, (c) FT-IR spectra of P5-COF before and after five cycles of adsorption study.

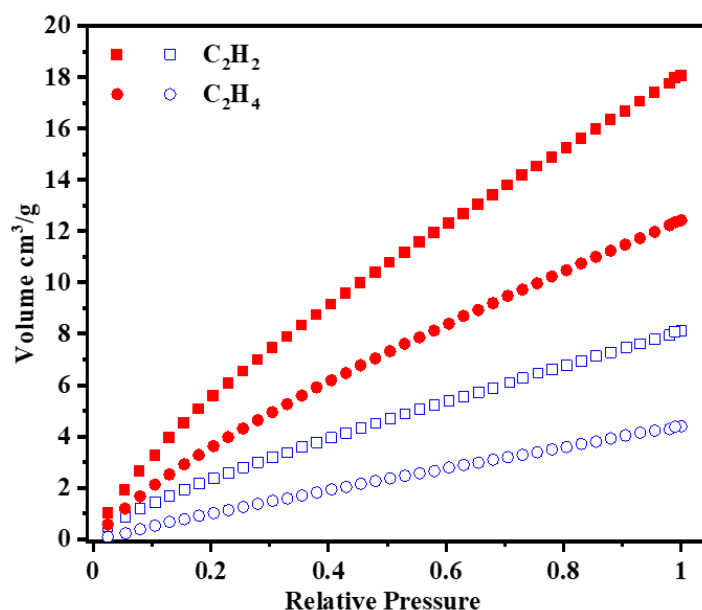


Fig. S17 Gas adsorption isotherms of **P5-COF** (red) and **Model-COF** (blue) at 295 K.

Table S2. Comparison of gas adsorption properties of **P5-COF** with other reported MOFs.

Adsorbents	C ₂ H ₂ uptake (cc g ⁻¹)	C ₂ H ₄ uptake (cc g ⁻¹)	C ₂ H ₂ /C ₂ H ₄ Selectivity (50:50)	Condition	Ref.
NPU-1	114	94	1.4	298K	J. Am. Chem. Soc., 2021, 143, 1485 - 1492.
NPU-2	90	77.2	1.25	298K	
NPU-3	57.7	49.7	1.32	298K	
SIFSIX-3-Ni	73.9	39.2	5.98	298K	Science, 2016, 353, 141 - 144.
SIFSIX-2-Cu	120.5	45.2	4.95	298K	
SIFSIX-1-Cu	190.4	92	8.37	298K	
Ni ₃ (pzdc) ₂ (7Hade) ₂	52.9	33.1	130	298K	Angew. Chem. Int. Ed. 2020, 59, 18927 - 18932.
HUST-5	50	38	1.8	273K	J. Mater Chem. A, 2020, 8, 2083 - 2089.
HUST-6	78	57	1.42	273K	
P5-COF	43	18	3.2	273K	This work
ZJNU-14	109.8	86.9	2.05	273K	Dalton Trans., 2020, 49, 15672- 15681.
P5-SOF	36	23	20	273K	Chem. Commun., 2017, 53, 6409 - 6412.

References:

- [1] S. Zhang, X.Li, W. Gong, T. Sun, Z. Wang and G. Ning, Pillar[5]arene-Derived Microporous Polyaminal Networks with Enhanced Uptake Performance for CO₂ and Iodine, *Ind. Eng. Chem. Res.*, 2020, **59**, 3269-3278.
- [2] L. Xu, Z. Wang, R. Wang, L. Wang, X. He, H. Jiang, H. Tang, D. Cao and B. Z. Tang, A Conjugated Polymeric Supramolecular Network with Aggregation-Induced Emission Enhancement: An Efficient Light-Harvesting System with an Ultrahigh Antenna Effect, *Angew. Chem. Int. Ed.*, 2020, **59**, 9908-9913.